Subsurface depth dependence of nitrogen doping in TiO_2 anatase: a DFT study

Shaida Anwer Kakil[1,2,*], Hewa Y. Abdullah[2,3],Tahseen G. Abdullah[1] and Nicola Manini[4,†]

[1] Department of Physics, College of Science Salahaddin University, 44001 Erbil, Iraq
[2] Research Center, Salahaddin University, 44001 Erbil, Iraq
[3] Physics Education Department, Faculty of Education, Tishk International University, 44001 Erbil, Iraq
[4] Dipartimento di Fisica, Università degli Studi di Milano, Via Celoria 16, 20133 Milano, Italy

E-mail: shaida.kakil@su.edu.krd* and nicola.manini@fisica.unimi.it†

Abstract. We report first-principles calculations of the structure and electronic structure of nitrogen-doped TiO_2 anatase as a function of the dopant depth below the (101) surface. Specifically we evaluate the depth dependence of the formation energy for a few positions of the N impurity, considering for both substitutional and interstitial sites. We find a significant advantage of interstitial over substitutional positions, and a mild dependence of this formation energy on depth. The lengths of the bonds surrounding the impurity also evolve smoothly with depth. Regarding the electronic structure, we report the main features of the intragap impurity states and the hole-related spin magnetization density surrounding the N impurity.

Keywords: N doping, anatase, spin magnetization

1. Introduction

In recent years numerous experimental and theoretical investigations of properties of titanium dioxide have been reported. This material has countless applications, for example in optoelectronic devices, including solar cells [1, 2], photon sensors [3], environment cleaning [4], and photocatalysis [5, 6, 7], just to mention a few. The doping of TiO_2 with nitrogen plays an important role in many of these applications because N dopants appear to enhance the photocatalytic activity of TiO_2 in the visible-light region through in-gap impurity levels. Nitrogen is a convenient dopant thanks to its atomic size comparable to that of oxygen, low cost and high stability [8, 9, 10].

In recent work, Di Valentin *et al.* [11] investigated the electronic and optical properties of TiO_2 modified by substitutional N-doping in the bulk. By state-of-the-art density functional theory (DFT) they showed that, in different crystalline structures and densities, N-doping has quite different effects. In particular, in the two main forms of TiO_2, anatase and rutile, it exhibits opposite effects on the photoactivity, leading to a red shift and a blue shift of the absorption edge, respectively. More recent simulations of nitrogen-doped anatase have advocated that under typical experimental conditions, nitrogen may prefer to substitute at a Ti-site [12]. However, this doping site has been ruled out by more recent experimental investigation [13], and we will not further consider it here.

Yang *et al.* [14] investigated the effects of the nitrogen concentration on the formation energies and electronic band structures of N-doped TiO_2 anatase on the basis of density functional theory (DFT) calculations. Wu *et al.* [15] used a DFT + Hubbard U method to investigate the influence of dopant concentration on the crystal structure, impurity formation energy, and electronic properties of N-doped anatase TiO_2, showing that heavy nitrogen doping of anatase results in the narrowing of the band gap and broadening the of the valence band. Ceotto *el al.* [16] studied the nitrogen location in nanocrystalline N-doped TiO_2 with a combined DFT and EXAFS approach: they evaluated the average Ti-nearest-neighbor distances, as obtained from EXAFS experiments and compared with DFT calculations at different levels of doping. They also showed that the creation of oxygen vacancies is observed at higher dopant concentration.

Tao *et al.* [17] carried out first-principles calculations of the magnetism and electronic structures for nitrogen-doped anatase TiO_2. They showed ferromagnetism in N:TiO_2 and attributed it to the hole-mediated double exchange through the strong p-p interaction between N and O. Spadavecchia *et al.* [18] carried out optical and electrochemical characterizations in conjunction with first-principles calculations on pure and N-doped titania nanocrystals showing that the position of the conduction band edge was not affected by doping, which rather introduces hole states in the band gap.

The optical properties of N doping are expected to be affected by the dopant distance from the crystal surface. It is therefore important to acquire a systematic understanding whether N impurities tend to reside at the surface layers of TiO_2 or

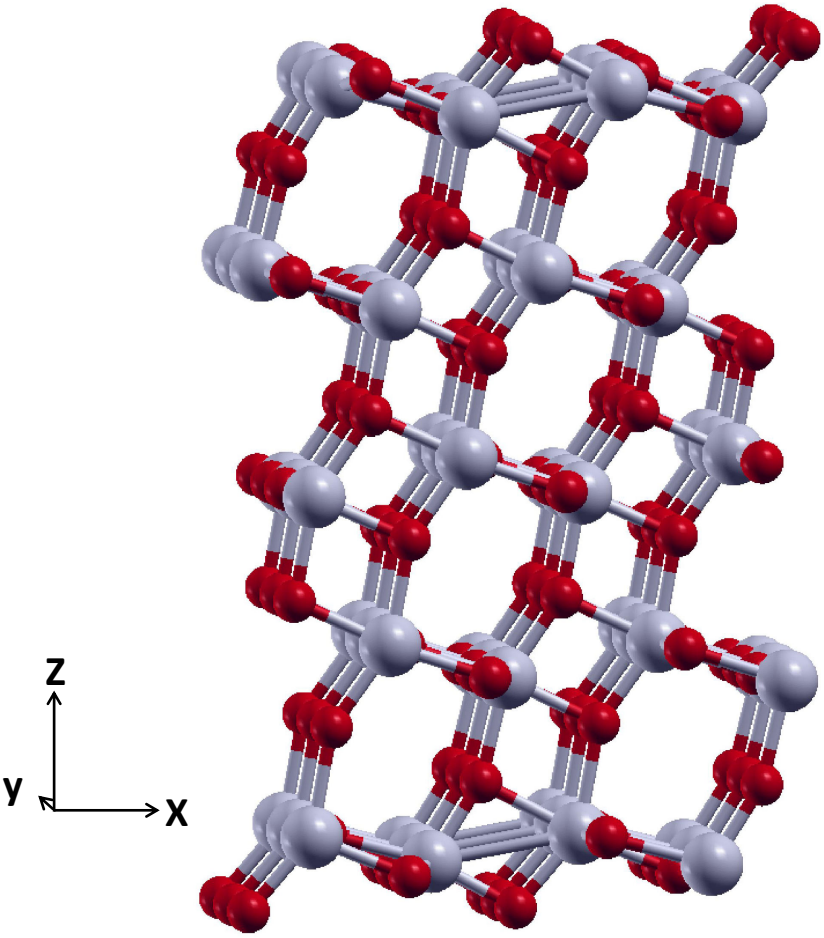

Figure 1. The 180-atoms supercell representing the slab model of the (101) surface of anatase TiO_2 considered in the present work.

rather deeper inside the bulk. While structural investigations of the pure TiO_2 (101) surface are available [19], we could not find any systematic investigation of the depth-dependence of the formation energy of N impurities in titania. For this reason, in the present paper we study the equilibrium structure, electronic structure, and magnetic properties of substitutional and interstitial N doping as a function of depth below the (101) surface of anatase, which is its most stable surface.

We adopt a symmetric slab geometry and carry out spin-polarized density-functional theory (DFT) calculations, for various positions of atomic nitrogen, changing its depth below the surface, testing both substitutional and interstitial doping. Our main result is that substitutional N doping exhibits slightly higher formation energy at locations near the surface than deeper in the bulk, while, for interstitial impurities, energetics favors marginally near-surface locations. Overall, the energy dependence on depth is modest.

To investigate the electronic structure of near-surface N-doped TiO_2 anatase, we adopt a standard slab geometry. We carve a five-layers, or 1.6 nm-thick, slab

out of bulk TiO_2 anatase, rotated in such a way that the $\hat{z}$ direction is aligned in the (101) crystallographic direction. In the horizontal $\hat{x}$ and $\hat{y}$ directions we adopt periodic boundary conditions. The supercell dimensions are $a = 1.040$ nm in the $(10\bar{1})$ crystallographic direction, aligned along $\hat{x}$, and $b = 1.136$ nm in the (010) direction, aligned along $\hat{y}$, resulting in a 1.182 nm^2 surface area of the model slab in the periodically-replicated supercell. The supercell contains 180 atoms. A 0.6 nm-thick layer of vacuum separates the slab from its periodic replicas in the $\hat{z}$ direction, to ensure the elimination of any interaction between adjacent slabs. The resulting supercell total size in the $\hat{z}$ direction is 2.2 nm. This model is depicted in Fig. 1.

On this structure, and doped variants thereof, we carry out multiple *ab-initio* DFT simulations using the plane-waves pseudopotential method as implemented in the Quantum Espresso package [20, 21]. For the exchange and correlation energy, we adopt a generalized gradient approximation (GGA), namely the Perdew-Burke-Ernzerhof (PBE) functional [22, 23]. We describe the core electrons via ultrasoft pseudopotentials [24]. The cutoffs for the plane-waves expansion of the Kohn-Sham wave functions and electron density are 50 Ry and 350 Ry, respectively. We sample the electronic band dispersion in the in-plane directions with 2×2 k points.

The comparison of the DFT total energy for the slab and for bulk anatase allows us to evaluate the surface energy of the (101) face of anatase. We estimate this surface energy to 0.48 J/m^2.

As nitrogen carries an odd number of electrons, and to take a better advantage of symmetry, we place two N atoms, one near each of the two slab surfaces. Of course, we stick to symmetry-equivalent sites. For each different position of the two N dopants in the TiO_2 anatase slab, we fully relax the structure, until the residual force on the atoms is less than 1×10^{-4} Ry/a_0. In each of these relaxed configurations, we evaluate the electronic structure, the total density of states (DOS), and the projected DOS (PDOS) on selected atoms. To account correctly for the spin of the unpaired electrons around the N dopants, we carry out spin-resolved calculations, thus obtaining the spin-density (i.e. magnetization density) spatial distribution.

In the described supercell, we consider six different substitution sites for nitrogen, at different depth. We label them as follows: N-N-1-T, N-N-1-M, N-N-1-B, N-N-2-C, N-N-2-M and N-N-2-B. The number (1 or 2) indicates the layer depth where substitution is performed. The T, M, B and C letter refers to the vertical position of the substituent atom within its layer, namely: T indicates top, C indicates center (a slightly less superficial position) M indicates middle, and B indicates bottom. All studied substitutional structures are depicted in Fig. 2.

To study interstitial N doping we compare four interstitial sites for nitrogen: two at the surface and two deeper in the slab, representative of the numerous possible locations. We label these structures as follows: I-N-N-1-T, I-N-N-2-T, I-N-N-1-B, and I-N-N-2-B. The letter "I" stands for interstitial. "T" means that the nitrogen sits near the top oxygen and "B" that the nitrogen sits near the bottom oxygen. The number indicates the depth of the layer near which the N impurity is inserted, counted from the surface.

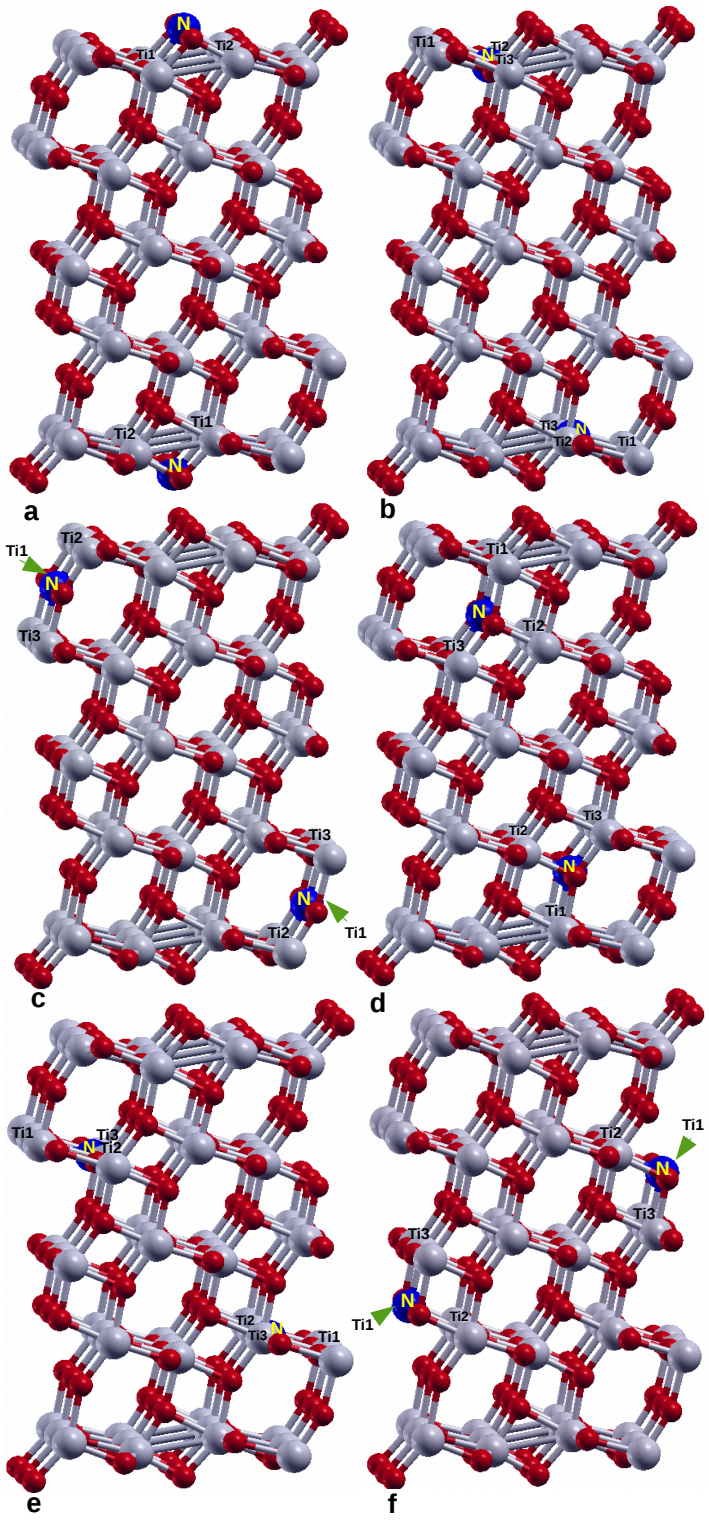

Figure 2. Optimized structures of the TiO_2 slab doped substitutionally at different sites. a: N-N-1-T, b: N-N-1-M, c: N-N-1-B, d: N-N-2-C, e: N-N-2-M, f: N-N-2-B. Gray and red balls stand for titanium and oxygen respectively. Blue balls represent the nitrogen dopants. Arrows indicate that a Ti atom bonded to the impurity is located across the cell periodic boundary.

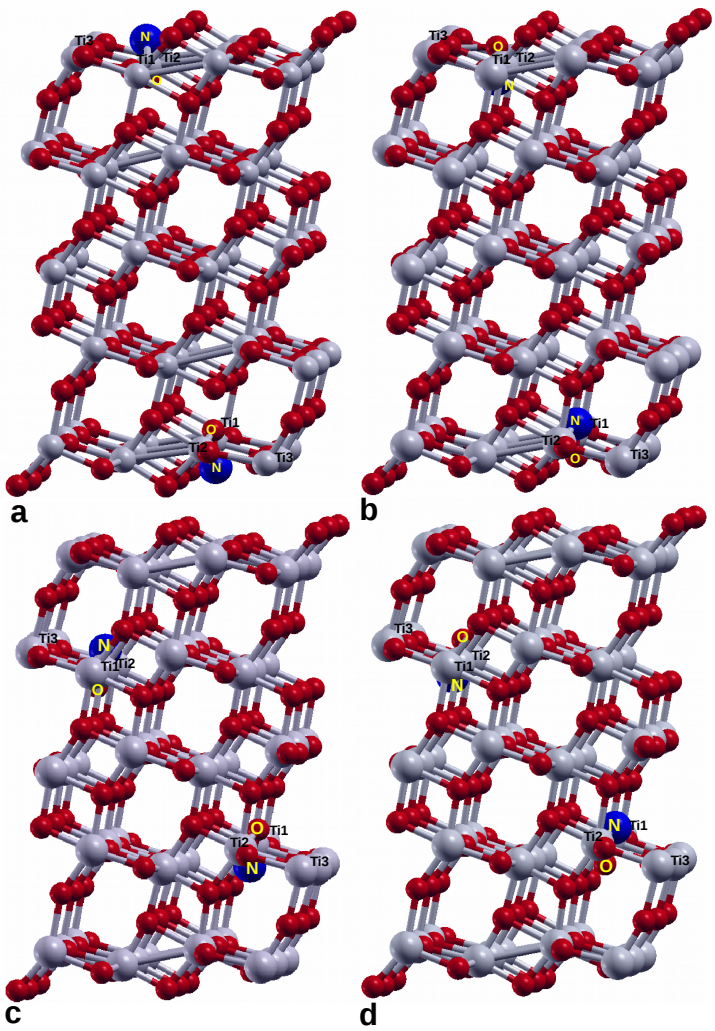

Figure 3. Optimized structures of interstitial-doped anatase TiO_2 at different sites relative to the (101) surface. a: I-N-N-1-T, b: I-N-N-1-B, c: I-N-N-2-T, d: I-N-N-2-B. Note that N atoms in interstitial positions form dimers with labeled O atoms of the anatase structure.

Figure 3 shows the considered interstitial arrangements.

The atomic positions of all relaxed atomic structures of N-doped TiO_2, as described and pictured above, are available as supplementary material [25].

2. Results and discussion

2.1. Bond lengths and formation energies: substitutional case

When the nitrogen substituents incorporate into the TiO_2 crystal, the Ti–N bond lengths are of course altered compared to the pristine Ti-O bonds. Table 1 reports the analysis of the bond lengths of the impurities as a function of the sub-surface depth. The two or three relevant impurity-metal bonds are labeled in Fig. 2. Based on our simulations, most bond lengths change by 1.5%–5%, with a few exceptions related to the B positions,

Table 1. Comparison of the bond lengths of substitional N-doped TiO_2 with the homologous bond lengths of the pure TiO_2 structure. All figures are in pm units. Individual bonds are identified in Fig. 2.

Label	O-Ti1	O-Ti2	O-Ti3	N-Ti1	N-Ti2	N-Ti3
N-N-1-T	185	183	–	194	193	–
N-N-1-M	206	194	194	216	196	196
N-N-1-B	210	178	202	214	186	202
N-N-2-C	212	196	191	210	207	197
N-N-2-M	202	194	194	210	196	196
N-N-2-B	186	200	200	192	209	200

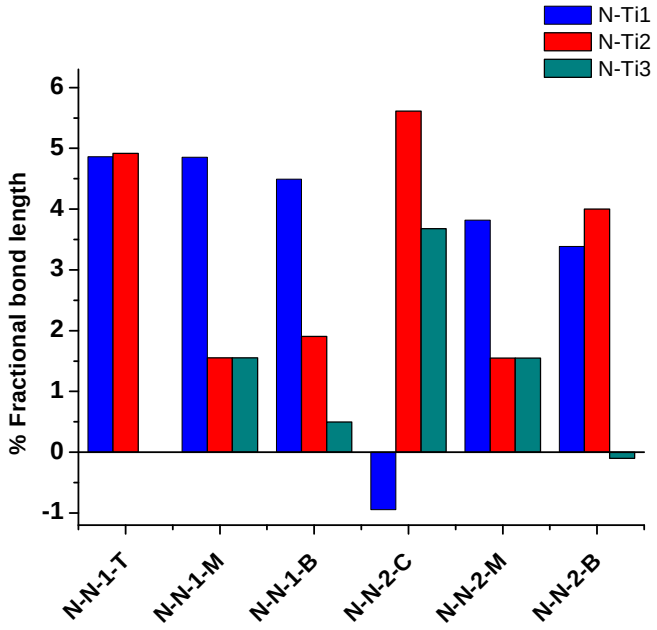

Figure 4. Fractional bond-length change of different substitutional positions of N dopants in TiO_2 for increasing depth below the (101) surface.

in both layer 1 and layer 2.

Previous research has studied the effect of doping on the bond lengths at the impurity site. Jin *et al.* [26] showed that in the bulk the Ti-N bond length is at least 1.5% longer than the regular Ti-O bonds of pure TiO_2. In their work, the bond lengths were also shown to change as a function of the nitrogen position.

Considering the bond lengths reported in Table 1 (see Fig. 2 for the labeling of N ligands of the individual substitutional configurations), we observe that, as is to be expected, the bonds formed by the near-surface substituents tend to elongate slightly more than those deeper down in the bulk, where structural constraints are more effective. To illustrate this observation, Fig. 4 reports the fractional bond length change of different substitutional N sites compared to the corresponding Ti-O bonds of pristine anatase.

To examine the stability of N-doped TiO_2 as a function of the sub-(101)-surface

Table 2. Impurity formation energies E_f, computed following Eq. (1), and the energy distance between the partly-filled impurity level and the top of the valence band $E_{IL} - E_{VB}$ of substitutional N-doped TiO_2.

N dopant position	$E_{\rm f}$ [eV] per dopant	$E_{IL} - E_{VB}$ [eV]
N-N-1-T	5.097	0.951
N-N-1-M	4.999	1.079
N-N-1-B	5.007	0.731
N-N-2-C	4.854	1.135
N-N-2-M	4.971	0.990
N-N-2-B	4.963	0.976

depth of the impurity the per-dopant formation energy for substitutional N doping in anatase $E_{\rm f}$ is calculated according to the following formula:

$$E_{\rm f} = \frac{1}{2}\left(E_{\rm 2N\,slab} - E_{\rm slab} + E_{\rm O_2} - E_{\rm N_2}\right), \tag{1}$$

where $E_{\rm 2N\,slab}$ and $E_{\rm slab}$ are the fully- relaxed total DFT energies of N-doped TiO_2 and pure TiO_2 in the slab structures depicted in Fig. 2 and Fig. 1, respectively. $E_{\rm N_2}$ and $E_{\rm O_2}$ are the energies of N_2 and O_2 in the molecular gas state, respectively. The factor 1/2 takes into account that the symmetric model slab involves two N dopants, one at each side.

Table 2 reports the resulting formation energies and the effective electronic gap energy $E_{IL} - E_{VB}$ between the lowest empty impurity level and the top of the valence band, for each of the configurations considered here. Previous works have also reported formation energies of doped TiO_2. Wu *et al.* [15] investigated the effects of nitrogen concentration on the formation energy of N-doped anatase TiO_2. Using a DFT + Hubbard U method, the formation energy of a N impurity in the bulk was evaluated to be 5.07 eV.

The formation energies computed according to Eq. (1) are listed in Table 2 for increasing depth below the (101) surface. When the dopant is located at the topmost surface layer (N-N-1-T, N-N-1-B, and N-N-1-M), the formation energy is slightly larger (more costly) than when the nitrogen sits deeper down in the bulk (N-N-2-M, N-N-2-C, and N-N-2-B), which is relatively surprising, in view of the stricter structural constraints. Overall, these positive formation energies are all quite large, indicating the scarce chemical affinity of TiO_2 for nitrogen. The mild dependence of $E_{\rm f}$ on depth suggests that a nonconstant substitutional-impurity depth-density profile, if any, is more likely to develop due to the formation kinetics of the doped crystal rather than to equilibrium thermodynamic mechanisms. If equilibrium effects play any role, they will tend to deplete the surface layer from substitutional N impurities, with a propensity of keeping them deeper inside the anatase crystal.

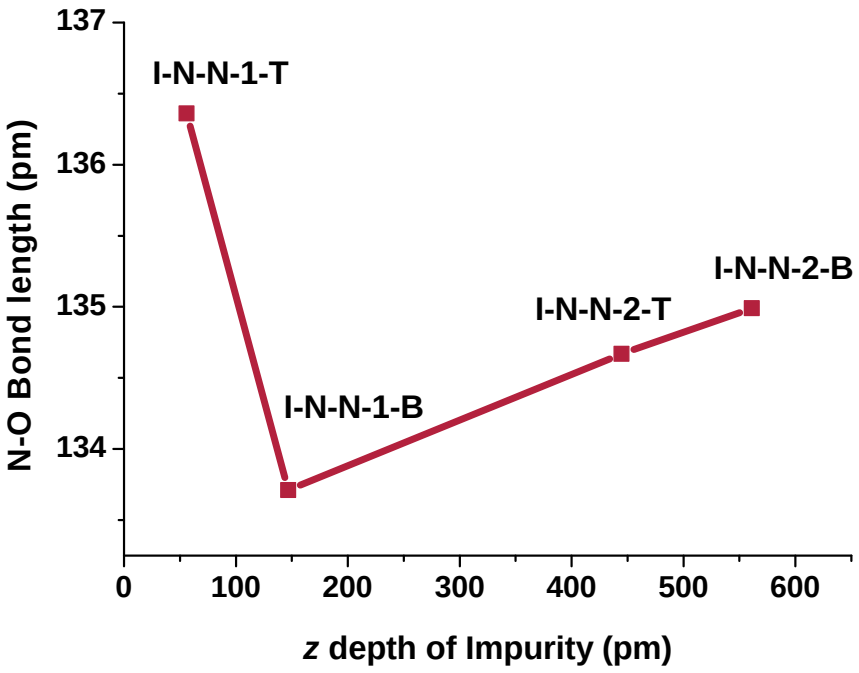

Figure 5. Bond length of the N-O dimer associated to interstitial N impurities, as a function of the depth of the N atom below the TiO_2 (101) surface.

Table 3. The lengths [pm units] of the bonds between N-O dimer formed by the interstitial impurity and the surrounding Ti atoms, as labeled in Fig. 3, as well as the N-O bond length, also reported in Fig. 5. Successive table entries are sorted for increasing depth of the dopant below the (101) surface.

Names of slabs	N-Ti1	N-Ti2	N-Ti3	O-Ti1	O-Ti2	O-Ti3	N-O
I-N-N-1-T	214	214	230	206	206	258	136
I-N-N-1-B	207	201	244	282	206	222	134
I-N-N-2-T	208	208	238	211	211	251	135
I-N-N-2-B	207	207	244	211	211	242	135

2.2. Bond lengths and formation energies: interstitial case

Interstitial N combines with O atoms in the anatase structure to form NO dimers. Figure 5 and Table 3 report the lengths of the relatively short bonds characterizing these N-O dimers for a few depths of the dopant at or below the TiO_2 (101) surface. Previous investigations [27] determined similar values for bulk doping, in the 136 pm region, compared with 115 pm of gas-phase NO. Overall, our results remain in substantial agreement with previous determinations, and indicate a mild dependence of the equilibrium bond length of this dimer on the sub-surface depth, with the longest bond occurring when the interstitial N sits right at the surface.

Table 3 reports also the lengths of the six bonds that the N interstitial atom and

Table 4. Formation energies $E_{\rm f}$, computed following Eq. (2), and the energy distance between the partly-filled impurity level and the top of the valence band $E_{IL} - E_{VB}$ of interstitial N-doped TiO_2, for increasing dopant subsurface depth.

Configuration label	$E_{\rm f}$ [eV]	$E_{IL} - E_{VB}$ [eV]
I-N-N-1-T	3.445	1.387
I-N-N-1-B	3.262	1.216
I-N-N-2-T	3.636	1.215
I-N-N-2-B	3.653	1.230

its paired O atom make to the three surrounding Ti atoms (indicated in Fig. 3), for increasing sub-surface depth of the dopant. Past research showed that the Ti-O and Ti-N bond lengths change in interstitial configurations, in particular as a function of the impurity concentration [28, 29, 30]. Shaoo *el at.* investigated these bond lengths experimentally, demonstrating an increase with increasing nitrogen concentration [31].

In our investigation, we explore how these bond lengths change as a function of the location and depth of the impurity, as reported in Table 3. These results indicate that also most of these bond lengths exhibit a relatively mild change with the impurity depth. In all configurations except for I-N-N-1-B, the dimer remains placed symmetrically between the Ti1 and Ti2 ligands. I-N-N-1-B marks an exception, in that a significant asymmetry is realized in the equilibrium state, with a tilted dimer; as a result, the oxygen atom forms a stronger shorter bond with Ti2 and a weaker and much longer bond with Ti1.

We evaluate the formation energy of interstitial configurations, too. We apply the following expression:

$$E_{\rm f} = \frac{1}{2}(E_{\rm 2N\,slab} - E_{\rm slab} - E_{\rm N_2}) \tag{2}$$

Compared to the substitutional case, we find a ~ 1.5 eV smaller energy, indicating that interstitial is the preferred location for N dopants. Contrary to the substitutional case, the formation energies of the interstitial dopant are smaller (less positive) at the surface than deeper inside the bulk. Figure 6 compares pictorially the depth dependence of the energetics of substitutional and interstitial N impurities.

2.3. Electronic properties of pure TiO_2 anatase

For a comparison with the doped configurations (discussed below), Fig. 7 reports the DOS and PDOS of TiO_2 anatase in its infinite bulk state, and for the (101) surface, in the slab model of Fig. 1. In addition to the total DOS, for both systems we report the projection on the p states of oxygen and the d states of titanium. To align the DOS and PDOS curves in different conditions, we always shift the bands so that the Fermi level sits at 0 eV. Consistently with other theoretical studies [32, 33, 34], the valence band edge of this material is dominated by O(2p), and the conduction band edge mainly involves Ti(3d) orbitals. The band gap for the slab, 2.315 eV is slightly

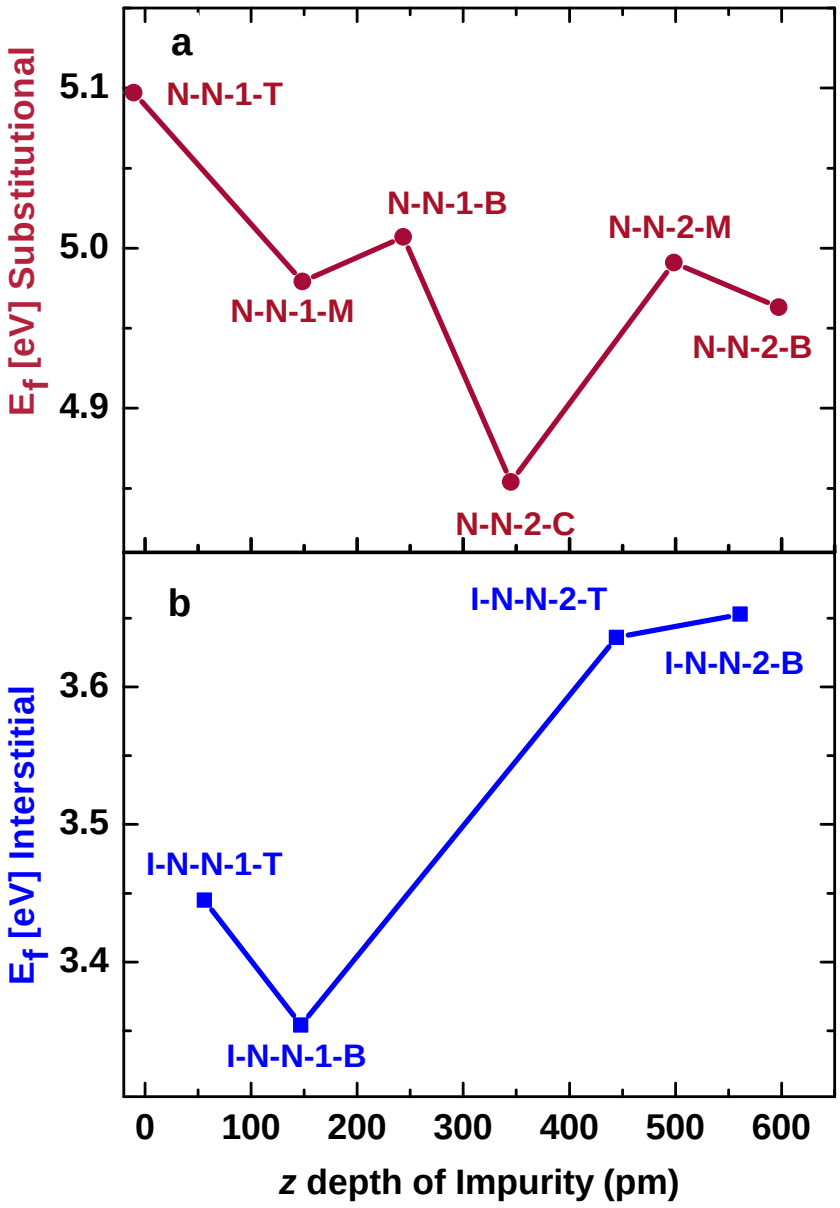

Figure 6. Formation energy as a function of the depth z of the N impurity below the (101) surface of anatase. (a): substitutional, structures of Fig.2; (b): interstitial, structures of Fig. 3.

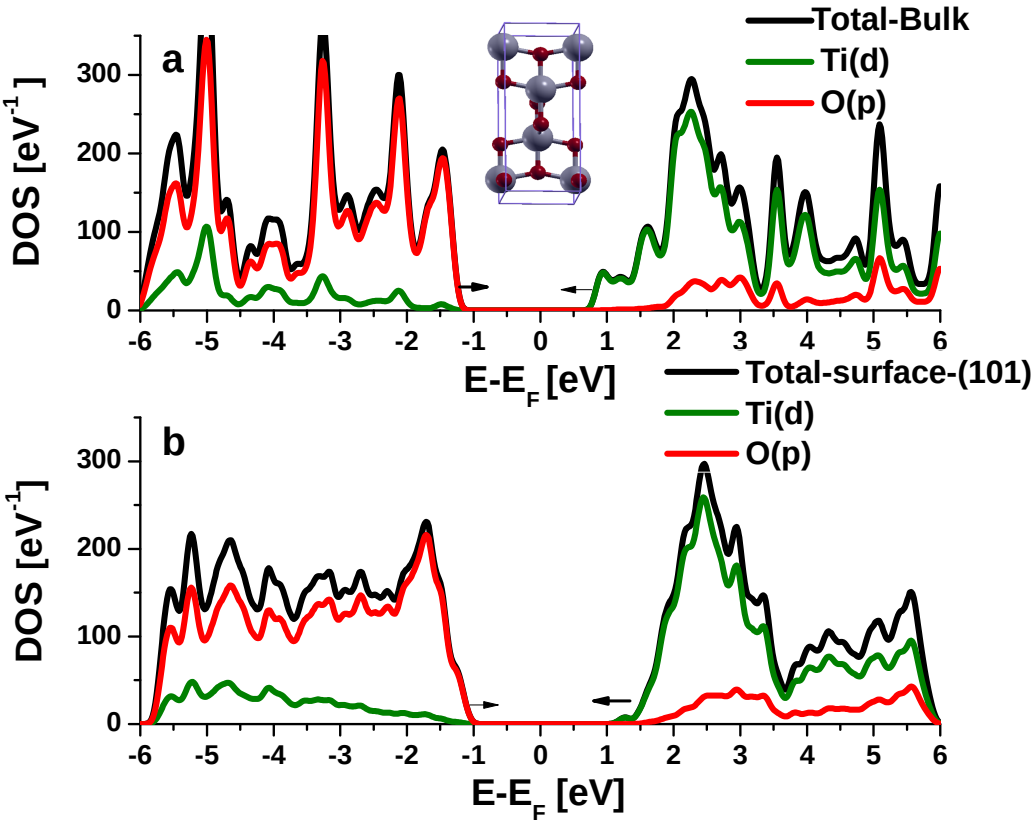

Figure 7. Density of states of pure (not doped) TiO_2 anatase. (a) The bulk crystal. (b) The (101) surface, described with the slab model of Fig. 1.

larger than $E_{CB} - E_{VB}$ obtained for bulk TiO_2 is 2.150 eV. This gap expansion is the consequence of an effective narrowing of the conduction band in slab calculations, which is a documented effect [23], also visible in Fig. 7.

The DFT gap we obtain is consistent e.g. with the work by Martsinovich *et al.* [23], where they report a gap of 2.12 eV which represent an underestimation of approximately 32% and 27% compared with the experimental value of 3.2 eV [35]. Underestimations in DFT calculations of band gaps are expected and documented due to well-known limitations of approximate DFT functionals [36]. The theoretical predicted energies of the empty impurity levels described below are also likely significantly underestimated, and only meant to provide qualitative trends. As in this work we are not specifically addressing optical properties of doped anatase, but rather structural properties, we are satisfied with the present level of theory.

2.4. Electronic properties for substitutional doping

To examine the effect of nitrogen doping on the electronic structure, we calculate the DOS and PDOS for different depths of the impurity. Figure 8 reports the DOS, comparing the pure TiO_2(101) surface with a few doping positions, as depicted in Fig. 2. Doping introduces deep impurity states inside the gap. N behaves as a p

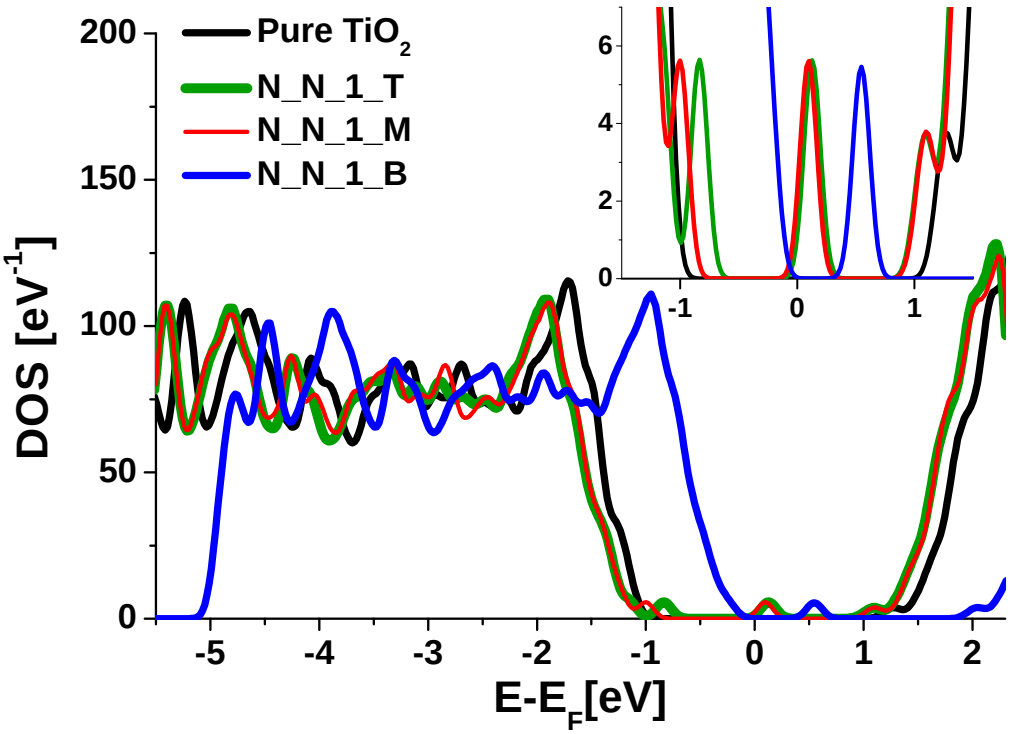

Figure 8. Comparison of the DOS for spin-up electrons of the pure and the doped TiO_2 (101) surface, at three locations of the substitutional dopant, see Fig. 2. The spin-down curves are identical. Inset: a blow-up of the gap region, highlighting the impurity states.

dopant [37, 38, 33], generating two impurity levels with similar wave functions: a lower, completely filled, one, which in all geometries remains within few meV of the valence-band maximum (VBM); and an empty hole state higher up in the bandgap. The energy separation between these two states, reported in Table 2 and visible in the inset of Fig. 8, changes significantly from one doping location to another, and it also results in displacements of the VBM relative to the intermediate Fermi level for the three reported DOS curves. Both states are delocalized π-bonding orbitals centered at the impurity and extending to two adjacent Ti ligands. The lower, filled, state is mostly localized in the plane defined by the impurity and the two Ti ligands, while the hole state has a node in this same plane. The different gaps are to be traced to different equilibrium Ti-N-Ti bond angles, which affect the splitting between these two extended π-bonding states, which would become approximately degenerate in the limit where the Ti-N-Ti angle reached 180°. For example, the N-N-1-B subsurface site relaxes to a remarkably large Ti2-N-Ti3 ligand angle (165°), accounting for the resulting record-low impurity-level separation of 731 meV, reported in Table 2 and by the blue curve in Fig. 8.

Figure 9 compares the spin-resolved DOS and PDOS of two nitrogen-doped configurations, those labeled N-N-1-B, namely the impurity in the surface layer, and N-N-2-B, with the impurity in the second layer deeper down, see Fig. 2. The PDOS identifies the states inside the gap as mainly N(2p) orbitals. The spin-resolved data in

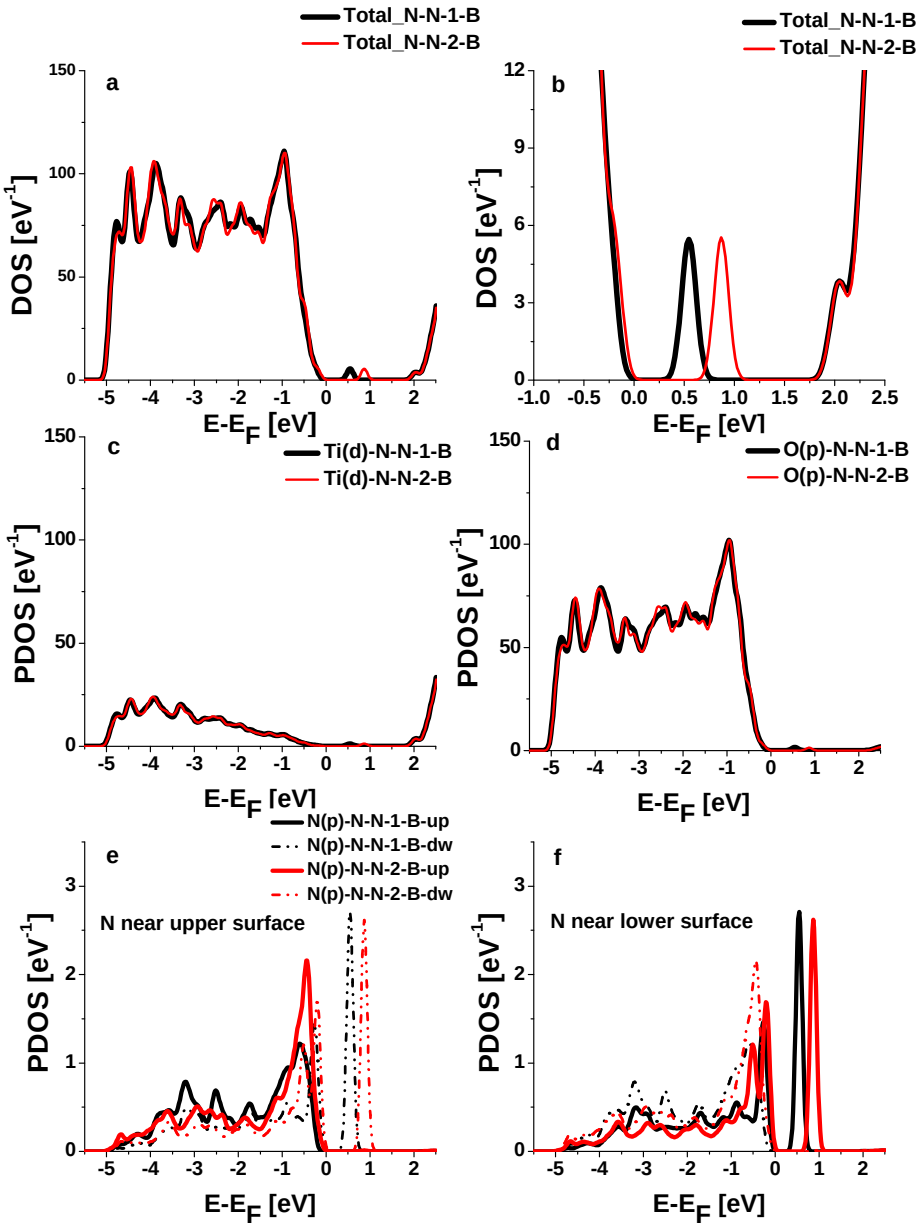

Figure 9. DOS and PDOS of substitutional N-doped TiO_2 anatase for dopant positions labeled N-N-1-B (in the surface layer) and N-N-2-B (one layer deeper), see Fig. 2. a: total DOS; b: detail of the gap and acceptor states; c: PDOS for Ti(d); d: PDOS for O(p); e: PDOS for the p projection at the N impurity near the upper surface; f: same as e, but for the lower surface, illustrating the antiferro spin alignment at the two impurities, which we obtain in all studied cases.

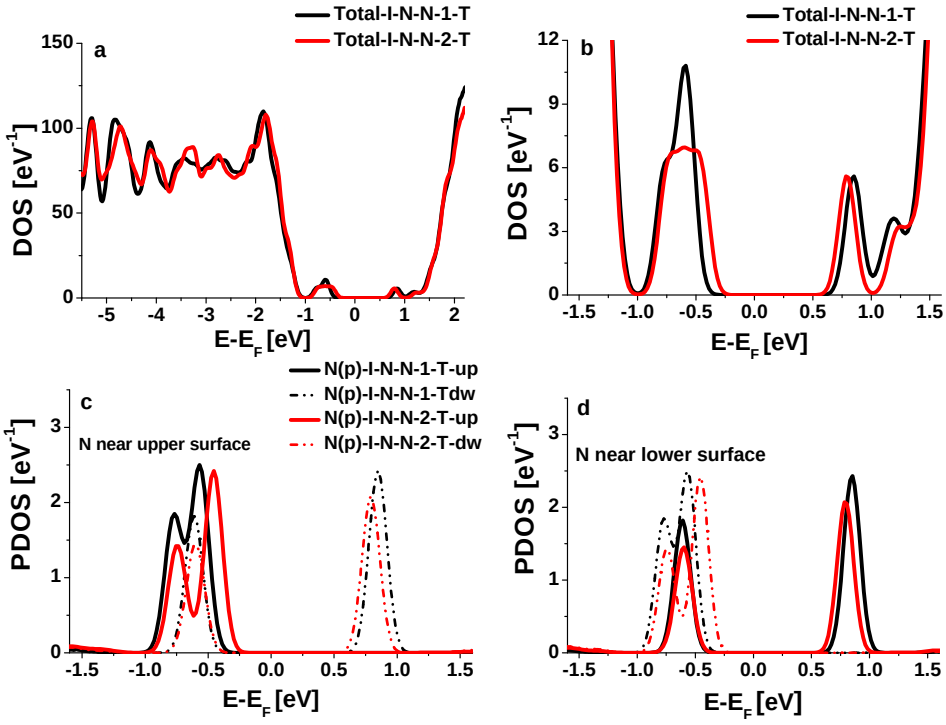

Figure 10. DOS and spin-resolved PDOS for interstitial-doped TiO_2 anatase, in the configurations labeled I-N-N-1-T (surface layer) and I-N-N-2-T (the second – deeper – layer), see Fig. 3. a: the total DOS; b: detail of the VBM and the impurity levels; c: the spin-resolved PDOS N(p) of the impurity near the upper surface; d: same but for the impurity near the lower surface.

Fig. 9e,f indicate that the magnetization of the localized states at the two impurities points in opposite directions, with the upper-surface impurity characterized by a predominantly spin-down electron density, and the lower-surface impurity characterized by a predominantly spin-up density. While this specific antiferromagnetic arrangement is a result of the adopted slab geometry, the fact that we obtain an antiferro ground state for all considered substitutional sites suggests that the spins carried by multiple N impurities in anatase should exhibit a general tendency toward antiferro mutual alignment, of standard superexchange nature.

2.5. Electronic properties for interstitial doping

Figure 10 shows the electronic properties of the interstitial N-doped surfaces, namely the I-N-N-1-T configuration (N atom in the surface layer) and I-N-N-2-T (N atom in the second layer). Compared with the substitutional case, we immediately notice the formation of two well-separated impurity levels in the gap. The lower, full level shows little or no magnetization, while the upper, empty one is fully spin-polarized. The gap between these localized levels is estimated to be in the 1.3 eV region, with small changes with depth. As the real gap is probably larger, it is likely to lead to near-infrared or visible-light absorption. These results are in line with previous research showing that

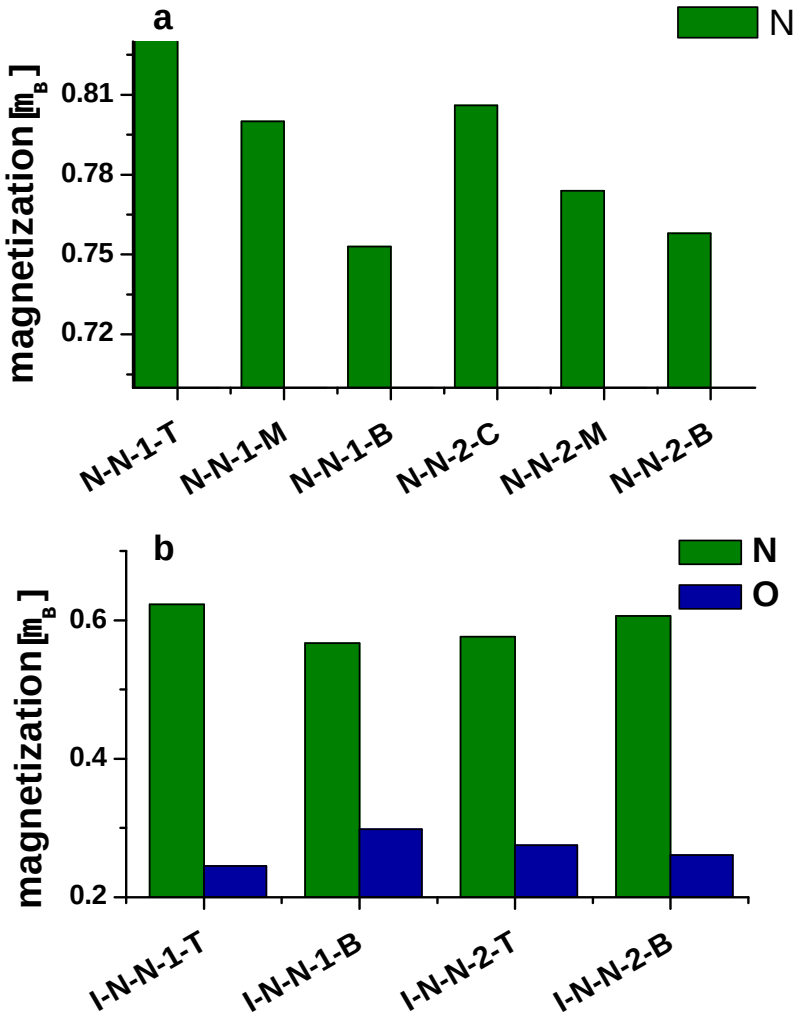

Figure 11. Total spin magnetization (units of μ_B at a N impurity in TiO_2, for different sub-surface depths. (a) Substitutional doping. (b) Interstitial doping, where O refers to the oxygen atoms forming a dimer with N. The structures of the individual labeled models are depicted in Figs. 2 and 3.

the photocatalytic activity of interstitial nitrogen-doped TiO_2 is higher than that of substitutional nitrogen-doped TiO_2 under visible-light illumination [39, 40, 41], although opposite claims have also been reported [37]. Here we find that the absorption peaks occur at different frequencies depending on the depth of the impurity relative to the anatase surface.

2.6. Spin magnetization

The extra impurity-related holes are responsible for the spin magnetization in the system. In our model doping with two nitrogen impurities, one near each surface of the slab, the resulting spin magnetization can arrange either symmetrically (ferro) or

antisymmetrically (antiferro) relative to the slab central symmetry plane. We check both possibilities and verify that in all cases the antisymmetric (antiferro) alignment of the spin magnetization is energetically favored compared to the symmetric (ferro) alignment.

For this antiferro electronic ground state, we compute the total magnetization around each atom by projecting the band wavefunctions of the two spin kinds on the atomic (pseudo)orbitals. This projection captures all but a very small (0.3%) component, which we neglect.

The total magnetization around each impurity is of the order of 1 Bohr magneton $\mu_{\rm B}$, and it decreases slightly with an increase in the depth of the impurity, as shown in Fig. 11a. Similarly, in the interstitial case shown in Fig. 11b the magnetization is slightly larger when the impurity is near the surface than when it is deeper down in the bulk. We also report the magnetization component in the oxygen partner of the interstitial impurity in the dimer: this oxygen collects some $0.2-0.3$ $\mu_{\rm B}$, thus a significant fraction the magnetization on the N atom itself. This result indicates a substantial delocalization of the hole in a molecular antibonding orbital of the dimer. This degree of delocalization changes with the impurity subsurface depth, and is especially significant in the I-N-N-1-B configuration, with the tilted dimer placed immediately below the surface atomic layer. In all configurations, all other oxygen and titanium atoms acquire quite small localized magnetic moments, which we do not report here.

To illustrate how the spin magnetization density arranges around the impurities, in Fig. 12 we present positive (yellow) and negative (pink) isosurfaces of the spin density, for two examples of near-surface impurity positions.

The substitutional case shown in Fig. 12a,c indicates a substantial localization of the magnetization density on the impurity atom, with a small spilloff to nearby O atoms and a tiny antiferro-correlated magnetization on nearest-neighbor Ti atoms. The interstitial case presented in Fig. 12b,d shows the magnetization associated with the previously-discussed hole shared between the N impurity and the dimer-partner O atom, with a small spilloff to nearby O atoms, and tiny antiferro-correlated contributions on the two Ti atoms closest to the dimer.

3. Discussion and Conclusions

We perform a spin-resolved DFT investigation of N doping near the anatase (101) surface. We consider both substitutional and interstitial doping for varied subsurface depths. Our main conclusions are as follows: (i) The analysis of the formation energy confirms that the interstitial positions are significantly favored energetically against the substitutional ones. (ii) Interstitial impurities slightly favor the immediate sub-surface position within the uppermost layer. By contrast, for substitutional doping, the depth dependence is quite mild, with positions deeper in the bulk slightly favored against those near the surface. (iii) The interstitial N forms a N-O dimer, and its bond length is shortest for the immediately sub-surface position, the tilted one with the lowest

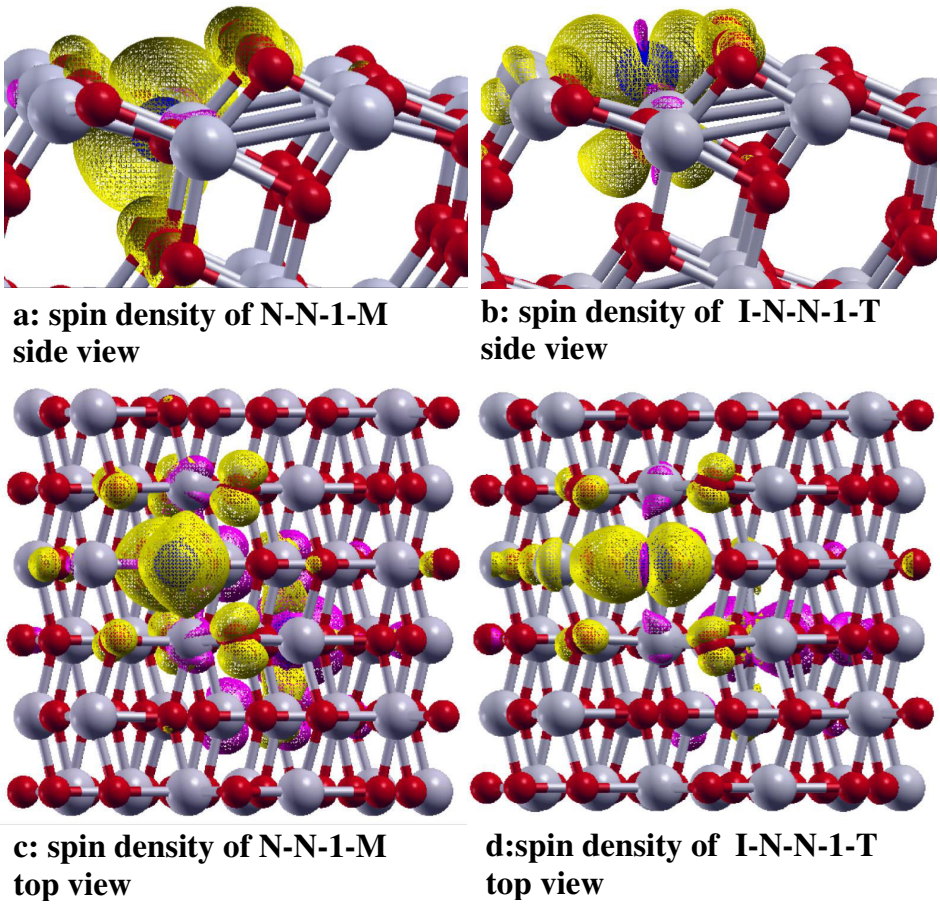

Figure 12. Side view (a and b) and top view (c and d) of two isosurfaces for the spin magnetization of (a and c) substitional, and (b and d) interstitial-doped TiO_2. Yellow/pink: spin magnetization level = $\pm 10^{-3}$ μ_B/a_0^3, i.e. $\pm 0.1\%$ atomic units.

formation energy.

In both interstitial and substitutional cases, the evaluated total-energy dependence is so mild that to reach a final conclusion about the thermodynamic properties of N impurities in anatase one should take other finer effects into account. At zero temperature, one should include differences in the zero-point vibrational energy. At finite temperature, one should also include entropic and enthalpic contributions, depending on the experimental conditions, such as partial pressure and chemical nature of the N-carrying reactants adopted in the doping process. Regardless of the outcome of these corrections, which are likely to depend rather mildly on depth as well, since energetics is quite flat as a function of depth the final structural positions of N impurities is likely to be determined by the kinetics in the doping process more than by equilibrium thermodynamics.

As for the electronic properties, for all doping configurations, impurity states appear between the valence band and the conduction band, with detailed energy positions

that depend on the impurity sub-surface depth and type. The obtained energetics and degree of localization of these states are most likely affected by the adopted DFT functional. A more accurate determination could be obtained by means of a suitable level of theory such as the GW approximation [42, 43] or DFT+U [44] or an hybrid functional including some amount of exact exchange [45]. Electron-spin resonance experiments could provide essential information about the magnetic properties of these localized states. These impurity levels can have important implications both for doping diagnostics and for applications when absorption in the visible region is needed, e.g. photocatalytic applications.

Acknowledgments

The authors acknowledge useful discussion with Elena Molteni, Guido Fratesi, and Cristiana Di Valentin, and acknowledge the grant HP10CGO446 for high-performance computer time at the national supercomputing center CINECA.

References

[1] Kim C W, Suh S P, Choi M J, Kang Y S and Kang Y S 2013 *J. Mater. Chem. A* **1** 11820
[2] Dharani S, Mulmudi H K, Yantara N, Trang P T, Park N G, Graetzel M, Mhaisalkar S, Mathews N and Boix P P 2014 *Nanoscale* **6** 1675
[3] Wang Y, Cheng J, Shahid M, Zhang M and Pan W 2017 *RSC Adv.* **7** 26220
[4] Ge M, Cao C, Huang J, Li S, Chen Z, Zhang K Q, Al-Deyab S S and Lai Y 2016 *J. Mater. Chem. A* **4** 6772
[5] Lee B H, Park S, Kim M, Sinha A K, Lee S C, Jung E, Chang W J, Lee K S, Kim J H, Cho S P, Kim H, Nam K T and Hyeon T 2019 *Nat Mater.* **18** 620
[6] Hussain H, Tocci G, Woolcot T, Torrelles X, Pang C L, Humphrey D S, Yim C M, Grinter D C, Cabailh G, Bikondoa O, Lindsay R, Zegenhagen J, Michaelides A and Thorntn G 2017 *Nat. Mater.* **16** 461
[7] Bettini L G, Dozzi M V, Foglia F D, Chiarello G L, Selli E, Lenardi C, Piseri P and Milani P 2015 *Appl. Catal. B Environ.* **178** 226
[8] Scanlon D O, Dunnill C W, Buckeridge J, Shevlin S A, Logsdail A J, Woodley S M, Catlow C R A, Powell M J, Palgrave R G, Parkin I P, Watson G, Keal T W, Sherwood P, Walsh A and Sokol A A 2013 *Nat Mater.* **12** 798
[9] Cho S, Ahn C, Park J and Jeon S 2018 *Nanoscal* **10** 9747
[10] Burda C, Lou Y, Chen X, Samia A C S, Stout J and Gole J L 2003 *Nano Lett.* **3** 1049
[11] Di Valentin C, Pacchioni G and Selloni A 2004 *Phys. Rev. B* **70** 085116
[12] Chen H and Dawson J A 2015 *J. Phys. Chem. C* **119** 15890
[13] Wojtaszek K, Wach A, Czapla-Masztafiak J, Tyrala K, Sá J, Özer L Y, Garlisi C, Palmisano G and Szlachetko J 2019 *J. Synchrotron Rad.* **26** 145
[14] Yang K, Dai Y and Huang B 2007 *J. Phys. Chem. C* **111** 12086
[15] Wu H C, Lin S W and Wu J S 2012 *J. Alloy. Compd.* **522** 46
[16] Ceotto M, Presti L L, Cappelletti G, Meroni D, Spadavecchia F, Zecca R, Leoni M, Scardi P, Bianchi C L and Ardizzone S 2012 *J. Phys. Chem. C* **116** 1764
[17] Tao J G, Guan L X, Pan J S, Huan C H A, Wang L, Kuo J L, Zhang Z, Chai J W and Wang S J 2009 *Appl. Phys. Lett.* **95** 062505
[18] Spadavecchia F, Cappelletti G, Ardizzone S, Ceotto M and Falciola L 2011 *J. Phys. Chem. C* **115** 6381

[19] Treacy J P W, Hussain H, Torrelles X, Grinter D C, Cabailh G, Bikondoa O, Nicklin C, Selcuk S, Selloni A, Lindsay R and Thornton G 2017 *Phys. Rev. B* **95** 075416
[20] Giannozzi P, Baroni S, Bonini N, Calandra M, Car R, Cavazzoni C, Ceresoli D, Chiarotti G L, Cococcioni M, Dabo I, Dal Corso A, de Gironcoli S, Fabris S, Fratesi G, Gebauer R, Gerstmann U, Gougoussis C, Kokalj A, Lazzeri M, Martin-Samos L, Marzari N, Mauri F, Mazzarello R, Paolini S, Pasquarello A, Paulatto L, Sbraccia C, Scandolo S, Sclauzero G, Seitsonen A P, Smogunov A, Umari P and Wentzcovitch R M 2009 *J. Phys.: Condens. Matter* **21** 395502
[21] Giannozzi P, Andreussi O, Brumme T, Bunau O, Buongiorno Nardelli M, Calandra M, Car R, Cavazzoni C, Ceresoli D, Cococcioni M, Colonna N, Carnimeo I, Dal Corso A, de Gironcoli S, Delugas P, DiStasio Jr R A, Ferretti A, Floris A, Fratesi G, Fugallo G, Gebauer R, Gerstmann U, Giustino F, Gorni T, Jia J, Kawamura M, Ko H Y, Kokalj A, Küçükbenli E, Lazzeri M, Marsili M, Marzari N, Mauri F, Nguyen N L, Nguyen H V, de-la Roza A O, Paulatto L, Poncé S, Rocca D, Sabatini R, Santra B, Schlipf M, Seitsonen A P, Smogunov A, Timrov I, Thonhauser T, Umari P, Vast N, Wu X and Baroni S 2017 *J. Phys.: Condens. Matter* **29** 465901
[22] Perdew J, Burke K and Ernzerhof M 1996 *Phys. Rev. Lett.* **77** 3865
[23] Martsinovich N, Jones D R and Troisi A 2010 *J. Phys. Chem. C* **114** 22659
[24] Vanderbilt D 1990 *Phys. Rev. B* **41** 7892
[25] See Supplementary Material, Document No. ??.
[26] Jin Y J, Linghu J, Chai J, Chua C S, Wong L M, Feng Y P, Yang M and Wang S 2018 *J. Phys. Chem. C* **122** 16600
[27] Di Valentin C and Pacchioni G 2014 *Acc. Chem. Res.* **47** 3233
[28] Zhao Z and Liu Q 2008 *J. Phys. D: Appl. Phys.* **41** 025105
[29] Lee S, Cho I S, Lee D K, Kim D W, Noh T H, Kwak C H, Park S, Hong K S, Lee J K and Jung H S 2010 *J. Photochem. Photobiol. A* **213** 129
[30] Chen H, Li X, RWana, Walter S K, Lei Y and Leng C 2018 *Chem. Phys. Lett.* **695** 8
[31] Sahoo M, Yadav A K, Jha S N, Bhattacharyy D, Mathews T, Sahoo N K, Dash S and Tyagi A K 2015 *J.Phys. Chem. C* **119** 17640
[32] Navas J, Sánchez-Coronilla A, Aguilar T, Hernández N C, de los Santos D, Sánchez-Márquez J, Zorrilla D, Fernández-Lorenzo C, Alcántara R and Martín-Calleja J 2014 *Phys. Chem. Chem. Phys.* **16** 3835
[33] Di Valentin C, Pacchioni G, Selloni A, Livraghi S and Giamello E 2005 *J. Phys. Chem. B* **109** 11414
[34] Long R and English N J 2011 *Chem. Phys. Lett.* **513** 218
[35] Dette C, Perez-Osorio M A, Kley C S, Punke P, Patrick C E, Jacobson P, Giustino F, Jung S J and Kern K 2014 *Nano Lett.* **14** 6533
[36] Landmann M, Rauls E and Schmidt W G 2012 *J. Phys. Condens. Matter* **24** 195503
[37] Zeng L, Song W, Li M, Jie X, Zeng D and Xie C 2014 *Appl. Catal. A* **488** 239
[38] Cheng X, Yua X, Xing Z and Wan J 2012 *Energy Procedia* **16** 598
[39] Peng F, Cai L, Yu H, Wang H and Yang J 2008 *J Solid State Chem.* **181** 130
[40] Asahi R, Morikawa T, Ohwaki T, Aoki K and Tag Y 2001 *science* **293** 269
[41] Livraghi S, Paganini M C, Giamello E, Selloni A, Di Valentin C and Pacchioni G 2006 *J. Am. Chem. Soc.* **128** 15666
[42] Hedin L 1965 *Phys. Rev.* **139** A796
[43] Giuliani G F and Vignale G 2005 *Quantum Theory of the Electron Liquid* (Cambridge Univ. Press)
[44] Hu Z and Metiu H 2011 *J. Phys. Chem. C* **115** 5841
[45] Becke A 1993 *J. Chem. Phys.* **98** 5648